Numerical simulation on thermal behavior of partially filled metal foam composite phase change materials

Qifan Ying, Hui Wang, Eric Lichtfouse

Applied Thermal Engineering 229 (2023) 120573

https://doi.org/10.1016/j.applthermaleng.2023.120573

Numerical simulation on thermal behavior of partially filled metal foam composite phase change materials

Qifan Ying [a], Hui Wang [a,b,*], Eric Lichtfouse [c]

[a] College of Environmental Science and Engineering, Donghua University, Shanghai 201620, China
[b] State Key Laboratory for Modification of Chemical Fibers and Polymer Materials, Donghua University, Shanghai 201620, China
[c] Aix Marseille Univ, CNRS, IRD, INRAE, CEREGE, Aix-en-Provence, France

Keywords:
Thermal energy storage
Phase change materials
Metal foam
Heat transfer enhancement
Partially filled

A B S T R A C T

As a kind of material with high thermal conductivity, metal foam embedded in phase change materials (PCM) can significantly improve the thermal energy storage performance of PCM, so as to better serve the latent heat thermal energy storage (LHTES). However, the presence of metal foam will suppress the natural convection of PCM, reduce its LHTES capacity and increase the total cost. In view of the above problems, this study designed LHTES units with metal foam filled at the top or the bottom with different height ratios. The melting heat transfer characteristic was studied by numerical simulations. Results show that the flow rate of liquid paraffin in the bottom filling configuration is one to two orders of magnitude higher than that in the top filling configuration, which plays a positive role in natural convection and is more conducive to heat transfer enhancement. However, the top filling configuration performs better in the heat storage capacity. The metal foam with a filling height ratio of 0.75 can increase the heat storage capacity by 7.47% while saving 25% material. On this basis, we proposed a new criterion, named the comprehensive strengthening goodness factor (CSGF), for evaluating the heat transfer performance of LHTES system. CSGF is different from the general criterion in that it can evaluate the heat storage capacity and the economic performance at the same time. Under the evaluation of CSGF, the optimum metal foam-paraffin configurations for different occasions were selected.

1. Introduction

Nowadays, saving energy consumption and exploring more efficient ways of energy utilization have become research hotspots [1,2]. Renewable energy resources, such as solar energy, is a popular way to store thermal energy. In thermal energy storage systems, the focus is on latent heat thermal energy storage (LHTES). This can be attributed to the fact that phase-change materials (PCM) being employed as heat storage media in the LHTES system, which can achieve a large amount of thermal energy storage within a small temperature difference [3]. In solar energy storage system, PCM is usually used to improve its intermittency and uneven spatial distribution [4,5]. In the electronic component thermal management system, it is used to absorb a large amount of heat emanating from electronic components and prevent high temperature damage [6,7].

The common types of PCM are generally organic, inorganic and eutectic. Many researchers have found that organic PCM has stable chemical and thermal properties, and compared with inorganic PCM, it is non-corrosive and has no phase segregation and super cooling phenomenon [8], which is a promising energy storage material in the future. However, due to the low thermal conductivity, the thermal energy storage effect is not up to expectations, so the application is limited. At present, methods to enhance the heat transfer of PCM mainly rely on external additives to strengthen, such as adding fins [9–12], Nanoparticles [13–16], graphene [17–20], and metal foam [21–24]. In these strengthening methods, metal foam is concerned. As summarized in Fig. 1, as a porous medium material, it has many obvious advantages such as small density, high surface area, high porosity and high thermal conductivity. This special skeleton interconnected network structure makes its heat transfer performance excellent. It combines well with PCM for wettability, and this metal foam composite phase change material has also been demonstrated to greatly enhance its heat transfer capability [25–30].

However, with the further research, it is found that metal foam can effectively enhance the melting heat transfer of PCM, but also bring some negative effects. Tao et al. [31] numerically studied the natural convection during the melting period of metal foam-paraffin composite

* Corresponding author at: College of Environmental Science and Engineering, Donghua University, Shanghai 201620, China.
E-mail address: huiwang@dhu.edu.cn (H. Wang).

Nomenclature

a	the weight coefficient of η_Q
A_m	Mushy coefficient
b	the weight coefficient of η_t
c	the weight coefficient of η_{pc}
c_p	Specific heat capacity ($J{\cdot}kg^{-1}{\cdot}K^{-1}$)
C_i	form coefficient (m^{-1})
d_f	fiber diameter (m)
d_p	pore size (m)
d_k	characteristic length (m)
f	liquid fraction
g	acceleration of gravity ($m{\cdot}s^{-2}$)
H	LHTES unit height (m)
H_{mf}	metal foam height (m)
i	unit price of metal foam ($\$·kg^{-1}$)
j	unit price of PCM ($\$·kg^{-1}$)
K	permeability (m^2)
L	latent heat of fusion ($kJ{\cdot}kg^{-1}$)
m	mass (kg)
M	unit price ratio of the metal foam to the PCM
Q	TES capacity (kJ)
S	source term
t	time (s)
t_m	melting time (s)
T	temperature (K)
T_m	melting point (K)
u, v	x,y direction velocity ($m{\cdot}s^{-1}$)
W	LHTES unit width (m)
x,y	Cartesian coordinates (m)

Greek symbols

α	thermal diffusivity ($m^2{\cdot}s^{-1}$)
γ	thermal expansion coefficient (K^{-1})
ε	porosity
λ	thermal conductivity ($W\ m^{-1}\ K^{-1}$)
μ	dynamic viscosity ($kg{\cdot}m^{-1}{\cdot}s^{-1}$)
ρ	density ($kg\ m^{-3}$)
ξ	height ratio of metal foam
η	value of the CSGF
δ	small constant number
χ	tortuosity coefficient
ω	pores per inch
ν	thermal energy storage rate ($kJ{\cdot}s^{-1}$)
θ	distance of deviation (m)

Subscripts

0	initial time
eff	effective value
pcm	phase change material
mf	Metal foam
l	liquid state
la	latent heat
s	solid state
se	sensible heat
w	wall

Abbreviations

BTC	bottom filling configuration
CSGF	comprehensive strengthening goodness factor
LHTES	latent heat thermal energy storage
PCM	phase change material
PPI	pores per inch
TES	thermal energy storage
TFC	top filling configuration

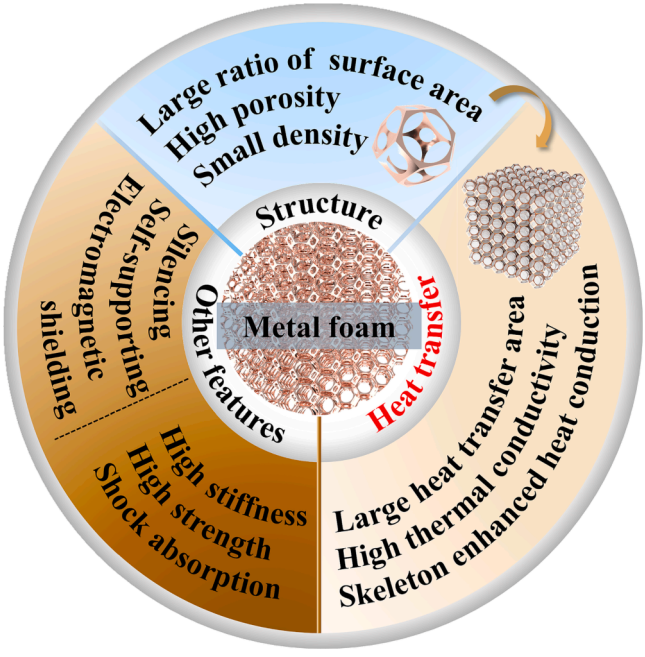

Fig. 1. Structural and performance advantages of metal foam.

materials. Results showed that the natural convection of paraffin was suppressed due to the obstruction of porous media, and this effect was enhanced at high pores per inch (PPI) with porosity greater than 0.9, which worsened the heat transfer. Lafdi et al. [32] pointed out that natural convection is beneficial to improve the uniformity of the temperature distribution of the composites, and the composites with high porosity and large pore size metal foam can reach the steady-state temperature faster, but the heat conduction decreases at the same time. Therefore, it is necessary to measure the strength of heat conduction and natural convection. Dinesh et al. [33] numerically simulated the total heat absorption and latent heat of composite materials (metal foams with different porosity), and found that the metal foams with low porosity enhanced the thermal conductivity of composite materials due to the presence of more metals, but inhibited the natural convection of paraffin in the pores and reduced the total heat absorption of paraffin. Mahdi et al. [34] recommended that metal foams with porosity greater than 0.9 in combination with paraffin wax, noting that metal foams with too low porosity will significantly reduce the volume of paraffin wax, resulting in less heat storage. These similar findings have been replicated in other studies [35,36]. It is known from previous studies that fully filled with metal foam will cause the natural convection and heat storage of PCM to weaken, and increase the cost. This makes partial filling an ideal way to allow more space for natural convection and heat storage, as well as lower costs. The excellent performance of finite metal foam filling is also confirmed [26,37,38].

Actually, the evaluation of the performance of this composite is based on both heat storage and material cost. However, the current study discusses the two separately. Joshi et al. [39] analyzed the influence of copper foam with different filling heights on the heat storage

performance of paraffin wax, and chosen the optimal filling strategy of copper foam based on the standard of reaching 90% of the heat storage of pure paraffin unit. Wang et al. [40] added metal foam of different mass into paraffin wax, and found that the heat storage and heat storage rate of composite materials showed opposite trends with the increase of the filling rate of metal foam. Taking these two factors into consideration, the filling rate at the intersection of these two curves is chosen as the optimal metal foam content. Xu et al. [38] proposed a heat storage performance evaluation index w for metal foam-paraffin composite units with different structures, which was defined as heat storage per unit mass per unit time. In the follow-up study, the economic performance evaluation index P_c is further proposed, which is defined as the heat storage of composite material per unit cost per unit time [41]. Lou et al. [42] carried out numerical simulation of ice storage spheres (metal foam-water) in the ice storage system, and used the above criteria (w, Pc) to determine the porosity of copper foam that makes the optimal cold storage performance and economic performance, respectively. Zuo et al. [43] also used dimensionless Pc' to investigate the economy of composite materials, and modified it under their research model. However, to the best of our knowledge, there is no evaluation criterion that considers both heat storage and economic performance.

Inspired by the finite metal foam filling strategy, LHTES units with two types of filling forms were designed in this study, top filling and bottom filling. Numerical simulation was carried out for different filling heights of metal foams under the two types of forms. The influence of the configuration on natural convection and heat storage was fully considered, and the performance evaluation of LHTES units was mainly studied. A new criterion was proposed to evaluate the heat storage and economic performance comprehensively. Based on which the optimal filling configuration and filling height ratio was obtained to provide reference for practical applications.

2. Physical model and numerical approach

2.1. Physical model

Fig. 2 shows the physical models of different filling configurations in this study. The size of the model (H × W) is 90 mm × 60 mm, in two-dimensional. The paraffin wax is used as the heat storage materials and copper foam is used for the enhanced heat transfer material. The two key parameters of copper foam are porosity and PPI. Porosity is defined as the ratio of the volume of pores in the metal foam to the total volume, which is taken as 90% in this paper. PPI is the number of pores per inch, and 10PPI is used in this paper. The thermophysical properties of paraffin wax and copper foam are listed in Table 1.

The filling ratio ξ is defined as the height of metal foam divided by the total height of the model. The left wall of the model is heated at a constant temperature, 423.15 K, other walls are adiabatic. Fig. 2(a) is the case without metal foam. Fig. 2(b) is the case fully filled with metal foam. Fig. 2(c) – (e) represents the cases partially filled with metal foam from the top and the filling ratio is 0.25, 0.5 and 0.75, respectively. Fig. 2(f) – (h) represents the cases partially filled with metal foam from the bottom. The filling ratio is also set to 0.25, 0.5 and 0.75, respectively. Fig. 3 shows the locations of the four the monitoring points. The distances of O_1, O_2, O_3 and O_4 from the bottom are 11.25, 33.75, 56.25 and 78.75 mm.

2.2. Equations

The enthalpy porosity approach and the volume averaging approach are employed to construct the numerical model presented in this study based on the following assumptions:

(1) The liquid PCM is considered incompressible and moves laminar, while its buoyancy effect follows the Boussinesq approximation.
(2) PCM and metal foam are isotropic.
(3) The thermophysical properties of PCM and metal foam are constant with various time, and they maintain local thermal equilibrium.

Based on the above premise, the governing equations can be written

Table 1
Thermo-physical properties of paraffin and copper foam.

	Paraffin	Copper
ρ (kg·m^{-3}) (Solid/liquid)	800/760	8930/-
c_p (J·kg^{-1}·K^{-1}) (Solid/liquid)	1800/2000	386/-
λ (W·m^{-1}·K^{-1})	0.24	398
L (kJ·kg^{-1})	250	–
(kg m^{-1}·s^{-1})	2.508 × 10^{-3}	–
γ (K^{-1})	7.5 × 10^{-4}	–
T_m (K)	318.15–328.15	–

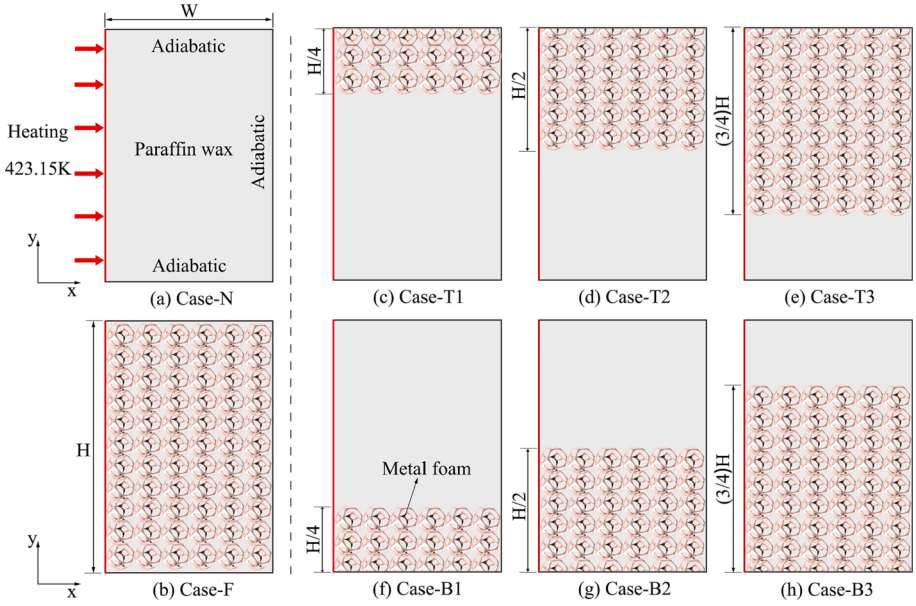

Fig. 2. Physical model of different configurations of metal foam in metal foam-paraffin systems.

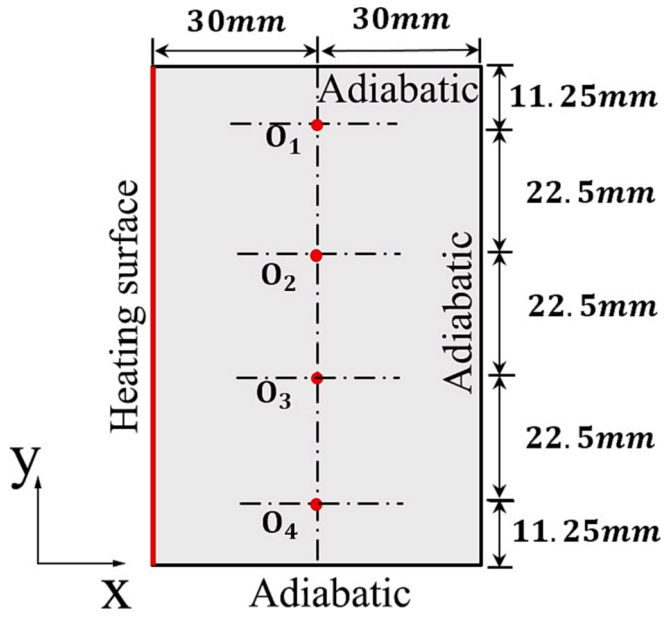

Fig. 3. Position of monitoring points.

as follows[44]:

Continuity equation:

$$\frac{\partial \rho_{pcm}}{\partial t}+\rho_{pcm}\left(\frac{\partial u}{\partial x}+\frac{\partial v}{\partial y}\right)=0 \tag{1}$$

Momentum equations:

$$\frac{\rho_{pcm}}{\varepsilon}\left(\frac{\partial u}{\partial t}+\frac{1}{\varepsilon}\left(\frac{\partial(uu)}{\partial x}+\frac{\partial(uv)}{\partial y}\right)\right)=-\frac{\partial p}{\partial x}+\frac{\mu_{pcm}}{\varepsilon}\left(\frac{\partial^2 u}{\partial x^2}+\frac{\partial^2 u}{\partial y^2}\right)+S_x \tag{2}$$

$$\frac{\rho_{pcm}}{\varepsilon}\left(\frac{\partial u}{\partial t}+\frac{1}{\varepsilon}\left(\frac{\partial(vu)}{\partial x}+\frac{\partial(vv)}{\partial y}\right)\right)=-\frac{\partial p}{\partial y}+\frac{\mu_{pcm}}{\varepsilon}\left(\frac{\partial^2 v}{\partial x^2}+\frac{\partial^2 v}{\partial y^2}\right)+S_y \tag{3}$$

S_x and S_y in Eqs. (2) and (3) are defined as momentum source terms in × and y directions, which can be expressed by the following formula:

$$S_x=-\frac{(1-f)^2}{f^3+\delta}A_m u-\left(\frac{\mu_{pcm}}{\mathrm{K}}+\frac{\rho_{pcm}C_i}{\sqrt{\mathrm{K}}}|u|\right)u \tag{4}$$

$$S_y=-\frac{(1-f)^2}{f^3+\delta}A_m v-\left(\frac{\mu_{pcm}}{\mathrm{K}}+\frac{\rho_{pcm}C_i}{\sqrt{\mathrm{K}}}|u|\right)v+\rho_{pcm}gf(T_{pcm}-T_0) \tag{5}$$

$$f=\begin{cases}0 T\le T_{m1}\\ (T-T_{m1})/(T_{m2}-T_{m1}) T_{m1}\le T\le T_{m2}\\ 1 T_{m2}\le T\end{cases} \tag{6}$$

The first term of S_x and S_y represents the flow resistance of PCM in the mushy zone when it is melted. f is the liquid fraction in the paraffin melting process, which is used to characterize the degree of melting process, and is a constant between 0 and 1. The higher the value, the more paraffin has been liquefied. 0 and 1 represent the completely solid and liquid cases, respectively [45]. δ is equal to 0.001 to avoid a zero denominator [46]. In addition, the coefficient A_m of the mushy zone is generally set to 10^5 [47–49]. T_{m1} and T_{m2} indicate the temperature of PCM in the solid and liquid state, respectively.

The remaining terms of S_x and S_y represent the changes in viscosity, inertia resistance and buoyancy caused by the metal foam. The parameters related to metal foam are calculated by semi-empirical correlations. K and C_i are the permeability and inertia coefficient of copper foam porous medium respectively, which can be obtained from the following equations [50].

$$\mathrm{K}=\frac{(\varepsilon d_k)^2}{36\chi(\chi-1)} \tag{7}$$

$$C_i=0.00212(1-\varepsilon)^{-0.132}\left(\frac{d_f}{d_p}\right)^{-1.63}/\sqrt{\mathrm{K}} \tag{8}$$

where χ, d_k, d_p and d_f are the tortuosity coefficient, characteristic length, pore size and fiber diameter of the metal foam respectively [51]. These are essential parameters to describe the structural characteristics of metal foams, and they directly determine the porosity and pore density of metal foams, which can be obtained from Eqs. (9)–(12).

$$\chi=2+2cos\left(\frac{4\pi}{3}+\frac{1}{3}cos^{-1}(2\varepsilon-1)\right) \tag{9}$$

$$d_k=\frac{\chi}{3-\chi}d_p \tag{10}$$

$$d_p=\frac{22.4\times10^{-3}}{\omega} \tag{11}$$

$$d_f=1.18\sqrt{\frac{(1-\varepsilon)}{3\pi}}d_p \tag{12}$$

Energy equation:

$$\left[(1-\varepsilon)(\rho c_p)_{mf}+\varepsilon(\rho c_p)_{pcm}\right]\frac{\partial T}{\partial t}+(\rho c_p)_{pcm}\left(u\frac{\partial T}{\partial x}+\frac{\partial T}{\partial y}\right)=\lambda_{eff}\left(\frac{\partial^2 T}{\partial x^2}+\frac{\partial^2 T}{\partial y^2}\right)-\varepsilon\rho L\frac{\partial f}{\partial t} \tag{13}$$

where, ε is the porosity of metal foam, the subscripts pcm and mf represent the phase change material (paraffin wax) and metal foam (copper) respectively, and λ_{eff} is the effective thermal conductivity of metal foam phase-change material composite, calculated by the model proposed by Bhattacharya [52]:

$$\lambda_{eff}=0.35(\varepsilon\lambda_{pcm}+(1-\varepsilon)\lambda_{mf})+\frac{0.65}{\left(\frac{\varepsilon}{\lambda_{pcm}}+\frac{1-\varepsilon}{\lambda_{mf}}\right)} \tag{14}$$

2.3. Boundary and initial conditions

The computation domain is shown in Fig. 2. During the melting period, the initial temperature of each filling configuration system is set to 293.15 K. All the four walls adopt the principle of none-slip, and the initial velocity in × and y directions is zero. The left wall is the heating surface, and the heating temperature is set to 423.15 K, which is a constant temperature heating method. The remaining three walls are defined as adiabatic to reduce heat loss. The junction between the composite and the pure paraffin regions were set as interior in the CFD program to ensure the heat and mass exchange between the two regions at the junction.

2.4. Numerical procedure

The governing equation is discretized by finite volume method (FVM) based on the double-precision solver. The SIMPLE algorithm is employed to handle the pressure–velocity coupling, and the pressure correction equation is discretized by the PRESTO method. Second order upwind algorithm is used in momentum and energy equations, and second order implicit algorithm is used in transient formulation. In addition, the residual convergence criteria for the continuity, the velocity and the energy equations are set at 10^{-4}, 10^{-4} and 10^{-6}, respectively.

3. Independence tests and model validation

3.1. Independence tests

In order to improve the accuracy of the numerical model and method, the number of grids and the time step were independently verified before model validation in this study. Through the analysis of the results, the optimal grid number and time step are selected to eliminate the errors caused by these factors and improve the computational efficiency. The independence test model is the case of a fully filled copper foam ($\varepsilon = 0.9$, 10PPI). The temperature of the left side wall is constant at 423.15 K, which is used as the heating surface, and the remaining wall is treated with adiabatic condition. The initial temperature of the LHTES unit is 293.15 K.

Firstly, the independence test was carried out on the grid numbers. The models with 5400, 10,564, 33,750 and 86,400 elements were selected respectively, and the time step was set as 1 s. The simulation results of the variations of liquid fraction with time under different gird numbers are shown in Fig. 4. With the increase of grid number, the process quickens sharply and then flattens out. In the case of 33,750 and 86,400 elements, although the number of grids is very different, the two curves overlap approximately, and the maximum deviation is only 0.73%, which is negligible. Considering the calculation accuracy and cost, the number of grid is determined as 33750, and the meshing is depicted in Fig. 5.

Secondly, under the condition that the grid number is 33750, the independence test is carried out for the calculation cases with time steps of 2 s, 1 s, 0.2 s and 0.1 s. Fig. 6 shows the simulation results of the variations of temperature with time at different time steps. Convergence can be achieved under each time step. When the time step is set to 0.2 s, the maximum deviation from the result of 0.1 s is only 1.1%. So a time step of 0.2 s is sufficient.

Finally, 33,750 was chosen as the optimum grid number, and the corresponding time step is 0.2 s.

3.2. Model validation

In order to verify the accuracy of the current numerical model, the numerical method in this study was used to deal with the PCM melting problem in porous media in the literature of Zheng et al. [53]. And compared with the simulation results. A square cavity of 60 mm × 60 mm was filled with paraffin and metal foam uniformly, and then the four operating conditions are simulated respectively on this basis. In Case-a,

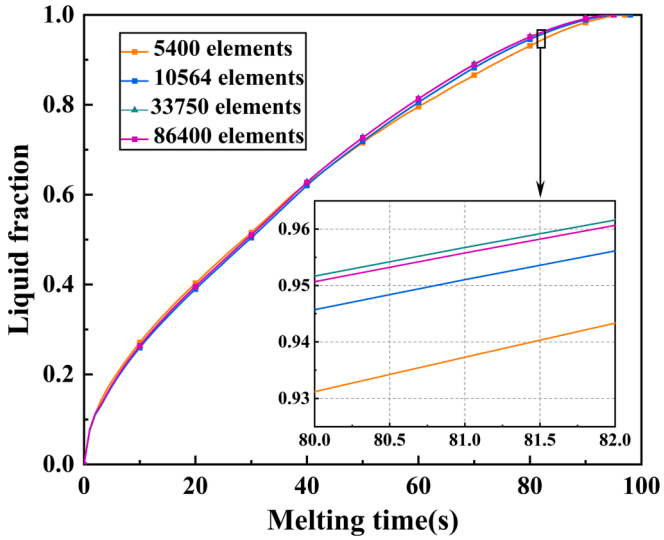

Fig. 4. Variations of liquid fraction with time for different grid numbers.

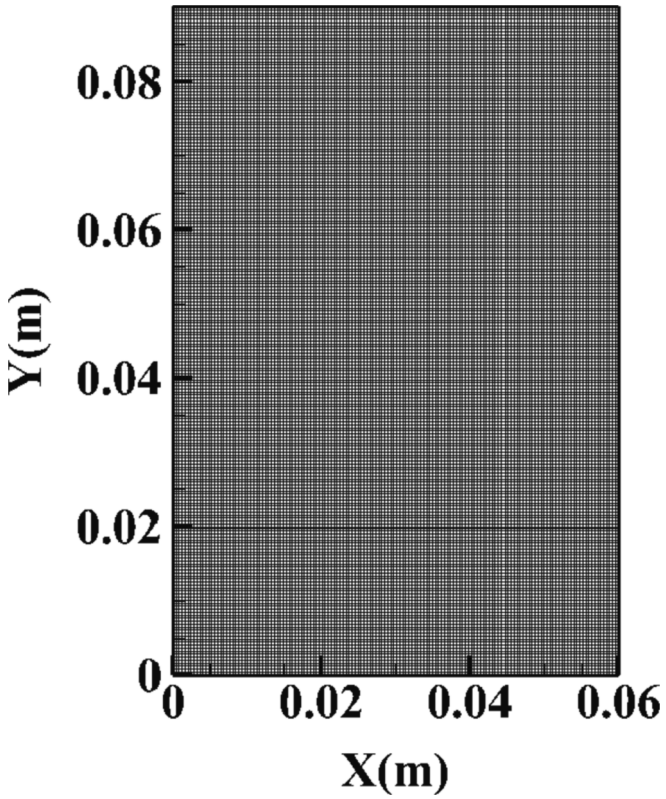

Fig. 5. Meshing system ($\xi = 1$).

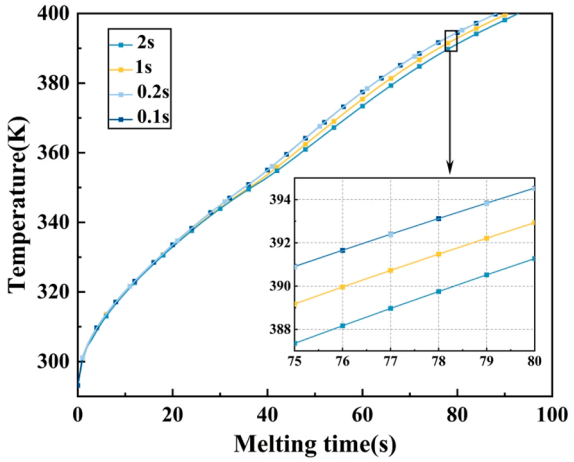

Fig. 6. Variations of temperature with time for different time steps.

nickel foam ($\varepsilon = 0.9$, 10PPI) was used, and a heating surface with a constant temperature of 350 K was located on the left side, while the rest of the wall was set as adiabatic. The remaining three cases used aluminum foam $\varepsilon = 0.95$, 10PPI) heated at a constant temperature from the bottom. The heating temperatures of Case-b, Case-c and Case-d are 350 K, 400 K and 450 K, respectively, and the other walls are insulated. The comparison results of liquid fraction with time are shown in Fig. 7. The simulation results under different operating conditions are in good agreement with the literature simulation results. The maximum error of the liquid fraction under the four operating conditions is 3.05%, which indicates that our numerical model is reliable.

In addition, the numerical results are compared with the experimental results of Li et al. [54]. A 100 mm × 45 mm × 100 mm three-dimensional cuboid model is established. The left wall is the heating

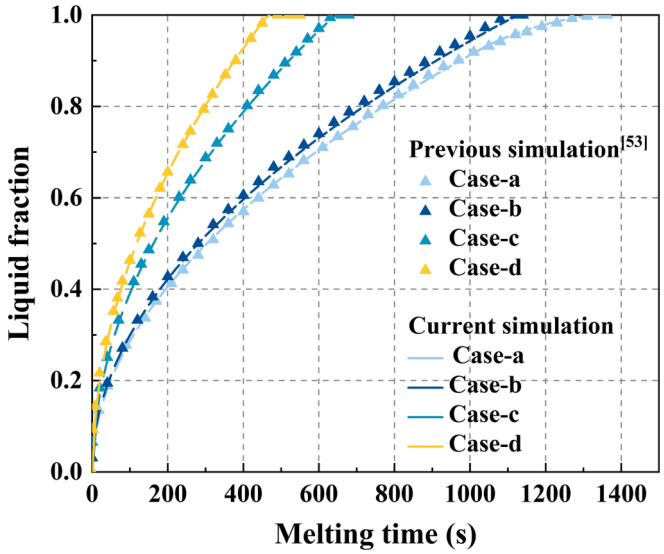

Fig. 7. Model validation results under the configuration of fully metal foam filled.

surface (constant heat flow: 4000 W/m^2), and the other walls are adiabatic. The melting temperature ranges from 319.63 k to 333.54 K, and the initial temperature is 299.15 K. The metal foam is made of copper ($\varepsilon = 0.9$, 10PPI). The model size and given conditions were set according to the literature experiment. In addition, a monitoring point with ×, y and z coordinates of 100 mm, 13 mm and 50 mm was established. The results are shown in the Fig. 8. It can be seen that the simulation results are in good agreement with the experimental data, and the maximum deviation is only 1.5%, which proves the reliability of the numerical method in this paper.

4. Results and discussion

4.1. Melting characteristics

4.1.1. Melting interface and temperature field

In order to better study the melt heat transfer mechanism under different filling configurations, the computational domain was divided into pure paraffin region and metal foam-paraffin region, and the liquid

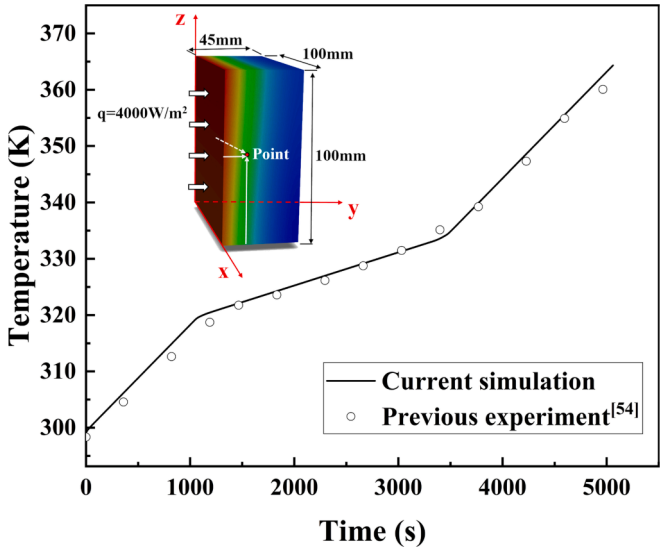

Fig. 8. Comparison of current numerical results with the previous experimental results.

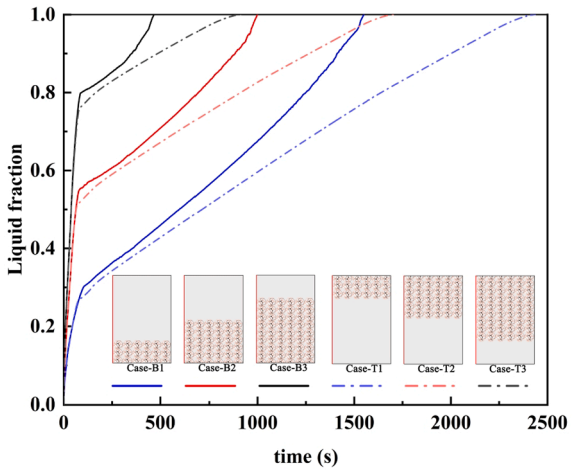

Fig. 9. The influence of different fillng configurations on liquid fraction.

fraction, melting interface, temperature field and velocity field in each region was discussed.

The liquid fraction changes and liquid–solid interface evolution of the two filling configurations are shown in Figs. 9 and 10, respectively. Fig. 9 shows the similar degree of liquefaction of the two configurations at the same metal foam filling height ratio (ξ). However, with the increase of ξ, the heat conduction was also enhanced, which accelerated the melting of paraffin in the composite region, so that more paraffin was melted at the same time and showed a higher liquid fraction. At the beginning of melting, the liquid fraction in each case develops linearly and has a high slope. This is because the paraffin in the composite region melts rapidly and thermal conductivity dominates heat transfer. For the two filling configurations, since ξ is the same, the liquid fraction curves almost coincide at the initial stage, which is proved in Fig. 10. Before 200 s, the liquid–solid interface of the two types of configurations in the pure paraffin and composite regions are similar. However, when the paraffin in the composite region melts, the development of liquid fraction takes a turning point. It can be seen that the liquid fraction of the bottom filling configuration has a steeper trend than that of the top filling configuration. This is because when the bottom is filled with metal foam, it acts as a heat source, and the melted hot paraffin moves from the left and bottom of the pure paraffin region to the top at the same time. As shown in Fig. 10, the melting interface shows a C-shaped movement to the right, which is similar to the phenomenon observed by Wang et al. [40] in the experiment. When the metal foam is filled at the top, it provides a top heat source for the pure paraffin region. However, due to natural convection, the high temperature liquid generated from the pure paraffin region will flow to the composite region. This, in turn, causes the pure paraffin region to lose heat and thus melt more slowly. As can be seen from Fig. 10, the melting interface of the top filling configuration slowly moves to the lower right corner.

Figs. 11 and 12 respectively show the influence of different configurations on temperature change and the temperature distribution at the time of melting completion. At the early melting stage, only trace paraffin close to the hot wall in the pure paraffin region melts, while in the composite region, due to the high thermal conductivity of the metal foam, the paraffin in this region rapidly heats up and liquefies. So in each case, temperatures rose quickly when the melting started. And with the increase of the metal foam, the more hot paraffin obtained after melting, so the unit reaches a higher average temperature. It can be seen from Fig. 11 that the average temperature of the top-filled configuration is higher than that of the bottom-filled configuration. This is because when the metal foam is located at the bottom, the heat of the high-temperature paraffin is absorbed by the pure paraffin region, making the average temperature lower. When the metal foam is at the top, the liquid paraffin accumulates in the composite region and gradually heats

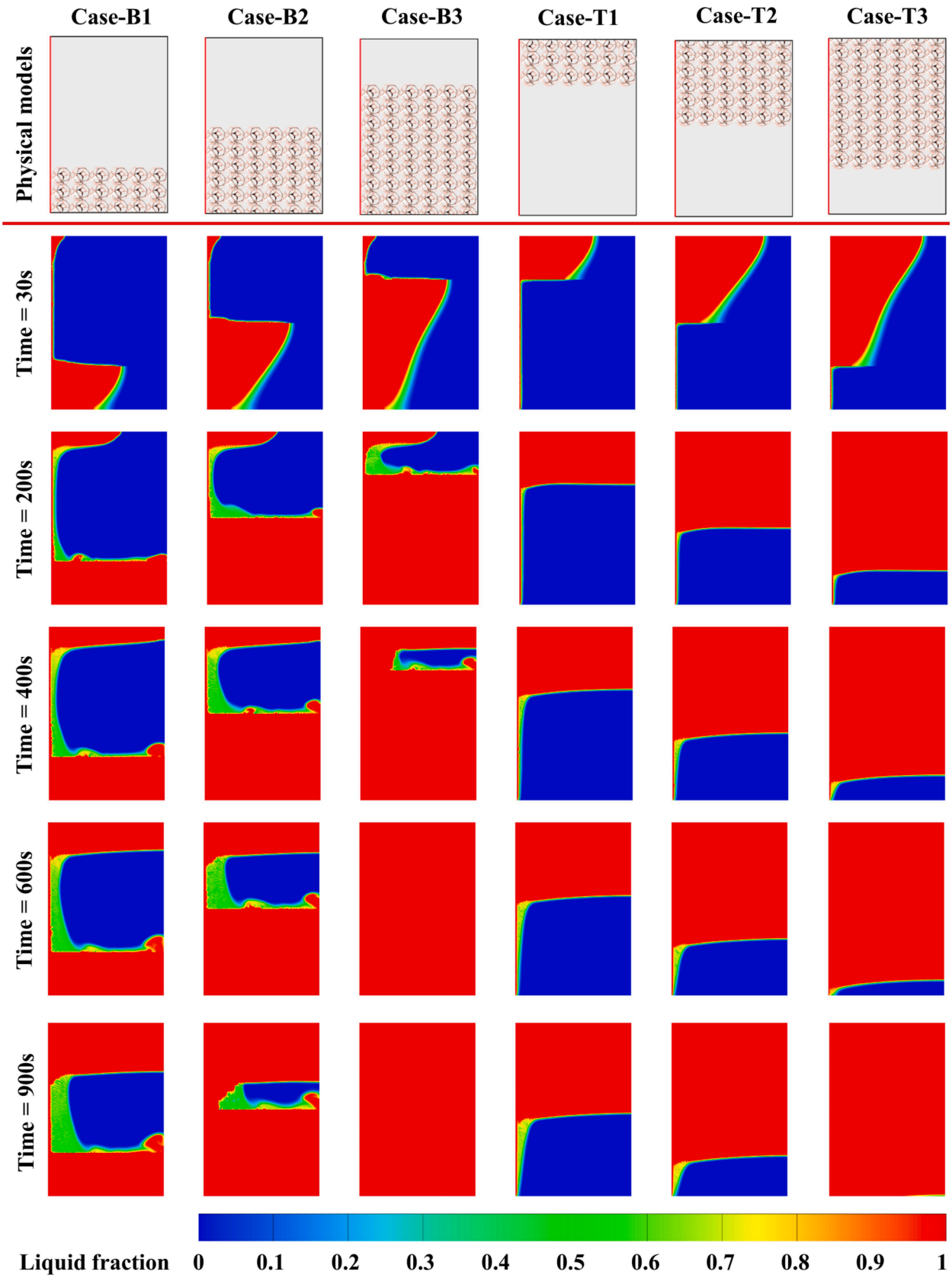

Fig. 10. Liquid-solid interface evolution of bottom-filled and top-filled configurations at different.

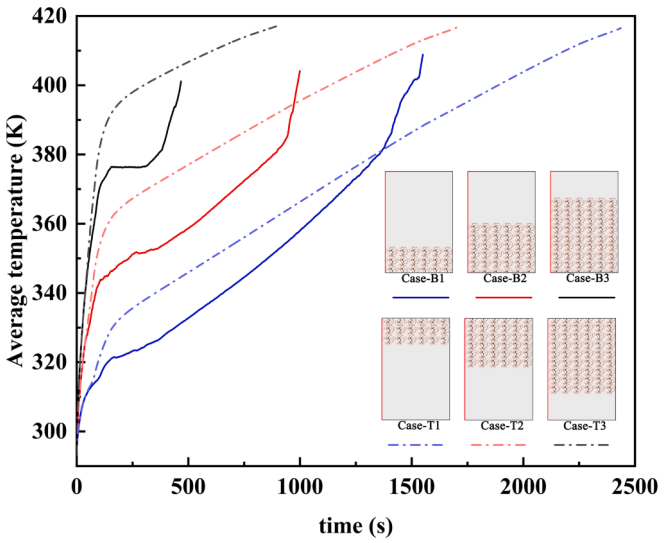

Fig. 11. Temperature distribution with melting time for different filling configurations.

up as it melts. The top filling and bottom filling configurations exhibit different temperature variations as the composite region melts. The pure paraffin region in the top filling configuration melts mainly by heat conduction, so the temperature rise rate is slow. However, natural convection was enhanced in this region with the bottom filling configuration, and the temperature rose at a higher rate in the later stage. However, due to the greatly shortened melting time, the temperature eventually reached was lower, which can be verified in Fig. 12.

It is found in Fig. 12 that the bottom temperature of each configuration is low, which is because the natural convection of paraffin transfers heat to the top portion, making it difficult for the bottom portion to melt. For bottom filling configuration, the temperature distribution becomes more uniform with the increase of metal foam. However, this is not obvious in the top filling configuration. Due to the longer melting time, there is little difference in the overall temperature. High temperature paraffin accumulates in the upper portion, and the temperature decreases from top to bottom with the development of melting. It can be seen from the liquid fraction and temperature change diagram that the melting rate and temperature rise rate of the bottom filling configuration are slightly higher than that of the top filling configuration. However, it is also obvious from Fig. 12 that the high temperature region of the top filling configuration is much greater, which can store more sensible heat.

4.1.2. *Velocity field*

The dimensionless time is defined as follows:

$$t^* = \frac{t}{t_m} \tag{15}$$

Where t_m is the complete melting time of the system. t is an arbitrary time during the melting process. The value of t^* is between 0 and 1.

Figs. 13-15 present the velocity field at different times for pure paraffin and the two types of filling configurations. In the pure paraffin region, each case had a vortex in the upper left corner at the initial stage of melting (before $t^* = 0.5$). That's because, the paraffin near the heating surface melts first. Under the action of buoyancy, the liquid paraffin flows upward, forming a vortex. However, the difference in the number of vortices in Figs. 14 and 15 is due to the location of the metal foam embedment. For the bottom filling configuration, because the metal foam accelerates the phase transformation process, there is a difference in temperature between the pure paraffin and the composite regions. This temperature imbalance results in two small vortices at the junction of the two regions, which located in the lower left and lower right corners of the pure paraffin region. The existence of the vortex zone is explained by the stable circulating flow of liquid, and the more vortices represent the stronger heat transfer. As the paraffin on the top portion is completely melted (after $t^* = 0.5$), the vortex originally located in the upper left corner moves down and joins the vortex in the lower left corner of the pure paraffin region, accelerating the melting process. However, for the top-filled configuration, despite the temperature difference at the junction of the two regions, liquid paraffin moved toward the composite region due to buoyancy, so there were no small vortices in the pure paraffin region as there were in the bottom filling configuration.

Table 2 shows the order of magnitude of velocity of liquid paraffin in different regions, which is similar to the order of magnitude of 10^{-4}m/s observed by Tian et al. [55] in the case of full metal foam filling. However, due to the different metal foam filling positions in this paper, some interesting phenomena were found. It is observed that the bottom filling configuration has a higher velocity in any region. The density of paraffin in the solid and liquid phases is different due to the different temperature, which flows upward under the action of buoyancy. With no metal foam on top, the liquid paraffin produced in the composite

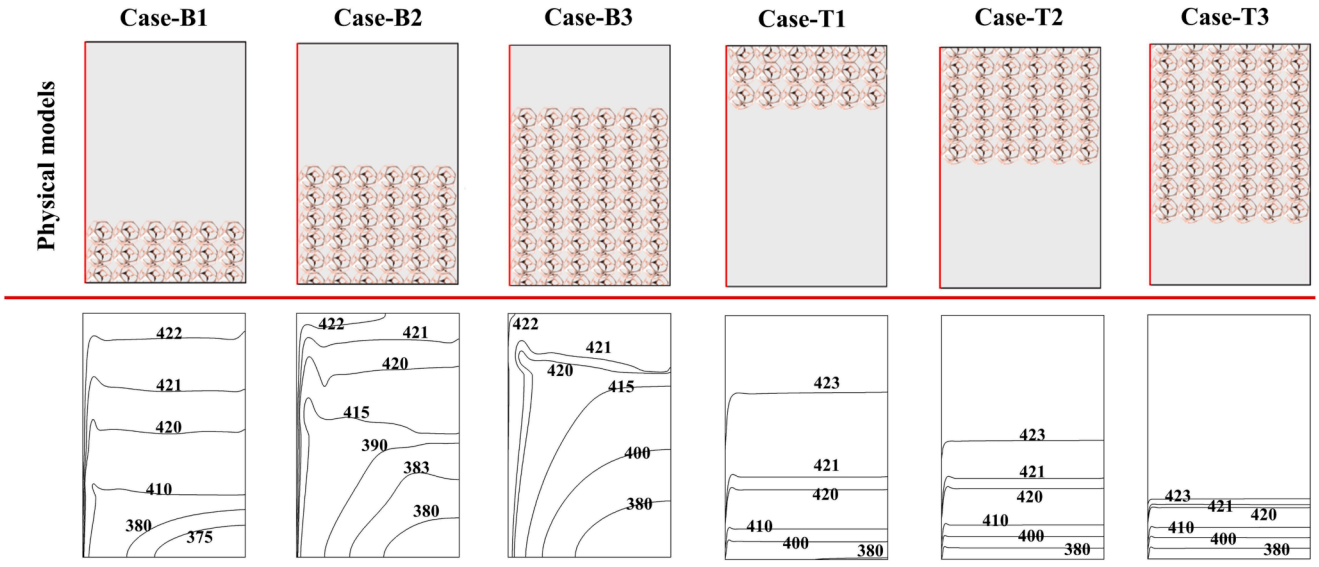

Fig. 12. Temperature distribution of each configuration at the time of melting completion.

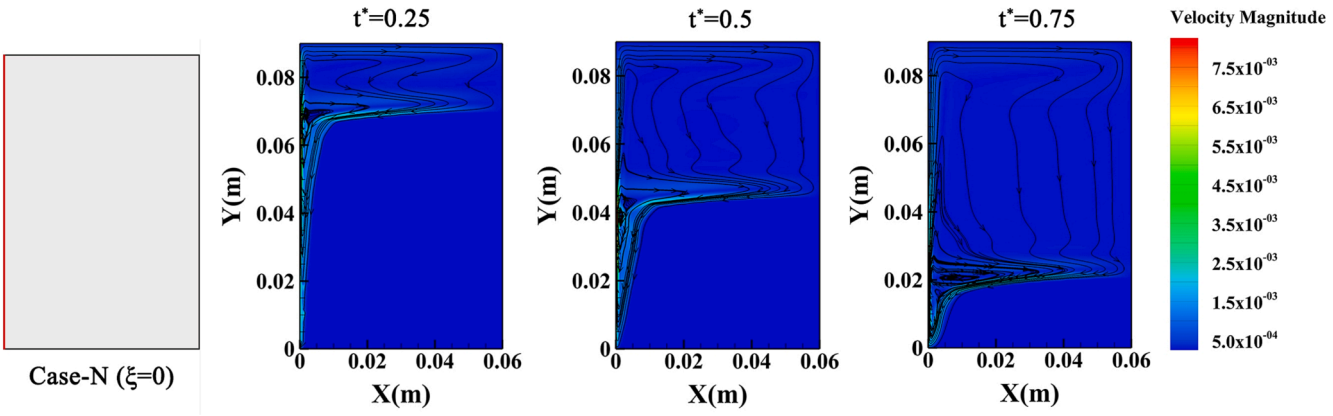

Fig. 13. Velocity field of pure paraffin(Case-N) at different times. The dimensionless time is 0.25, 0.5 and 0.75, respectively.

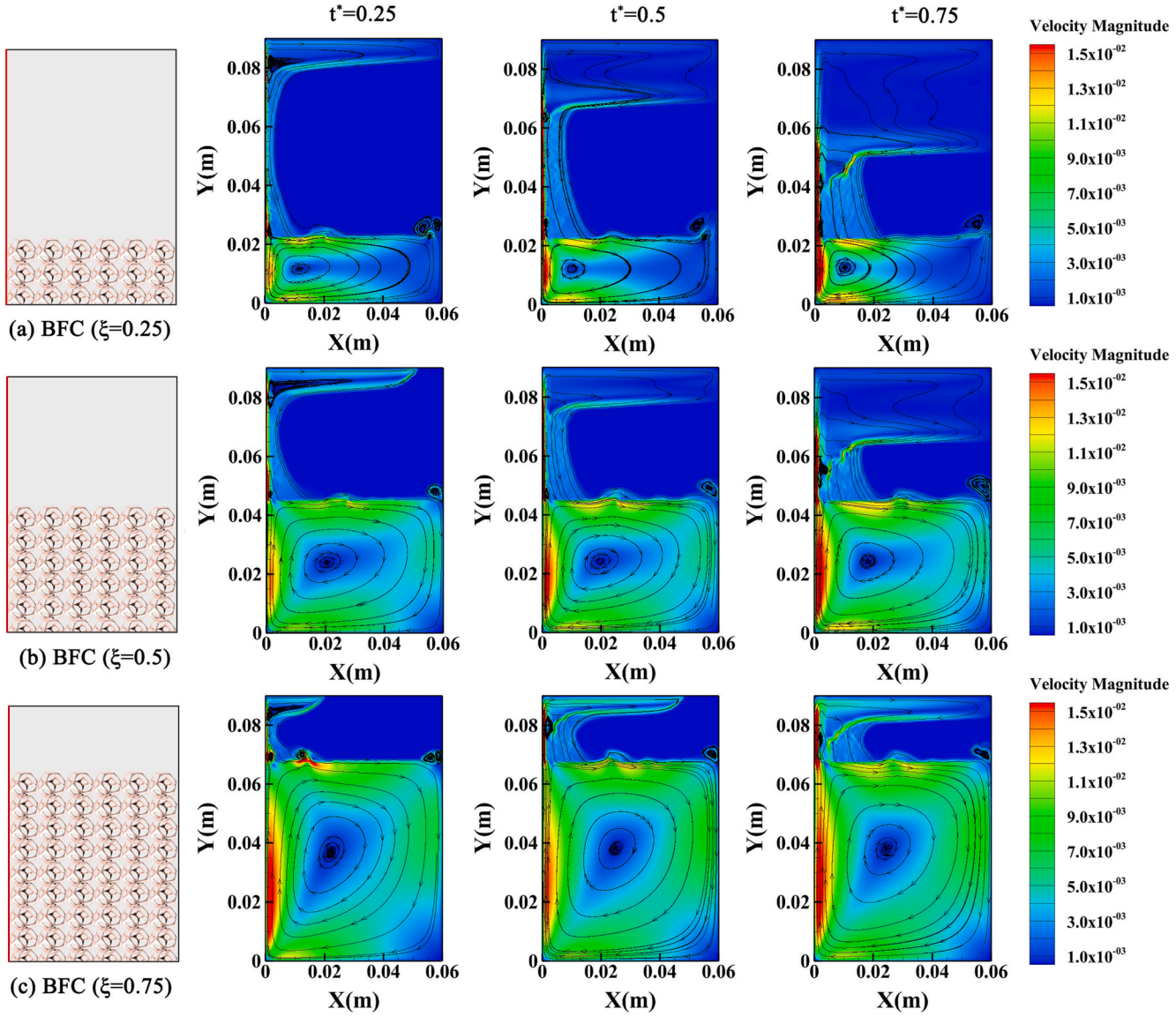

Fig. 14. Velocity field of the bottom filling configuration at different times. The dimensionless time is 0.25, 0.5 and 0.75, respectively.

region flows upward easily. Therefore, the flow velocity of the paraffin in the composite region is increased, which also strengthens the natural convection in the pure paraffin region and increases the flow velocity in this region. So it is reasonable to observe an order of magnitude of 10^{-3}m/s, greater than 10^{-4}m/s, in the composite region. The velocity in the pure paraffin region is on the order of 10^{-4}m/s, slightly larger than the

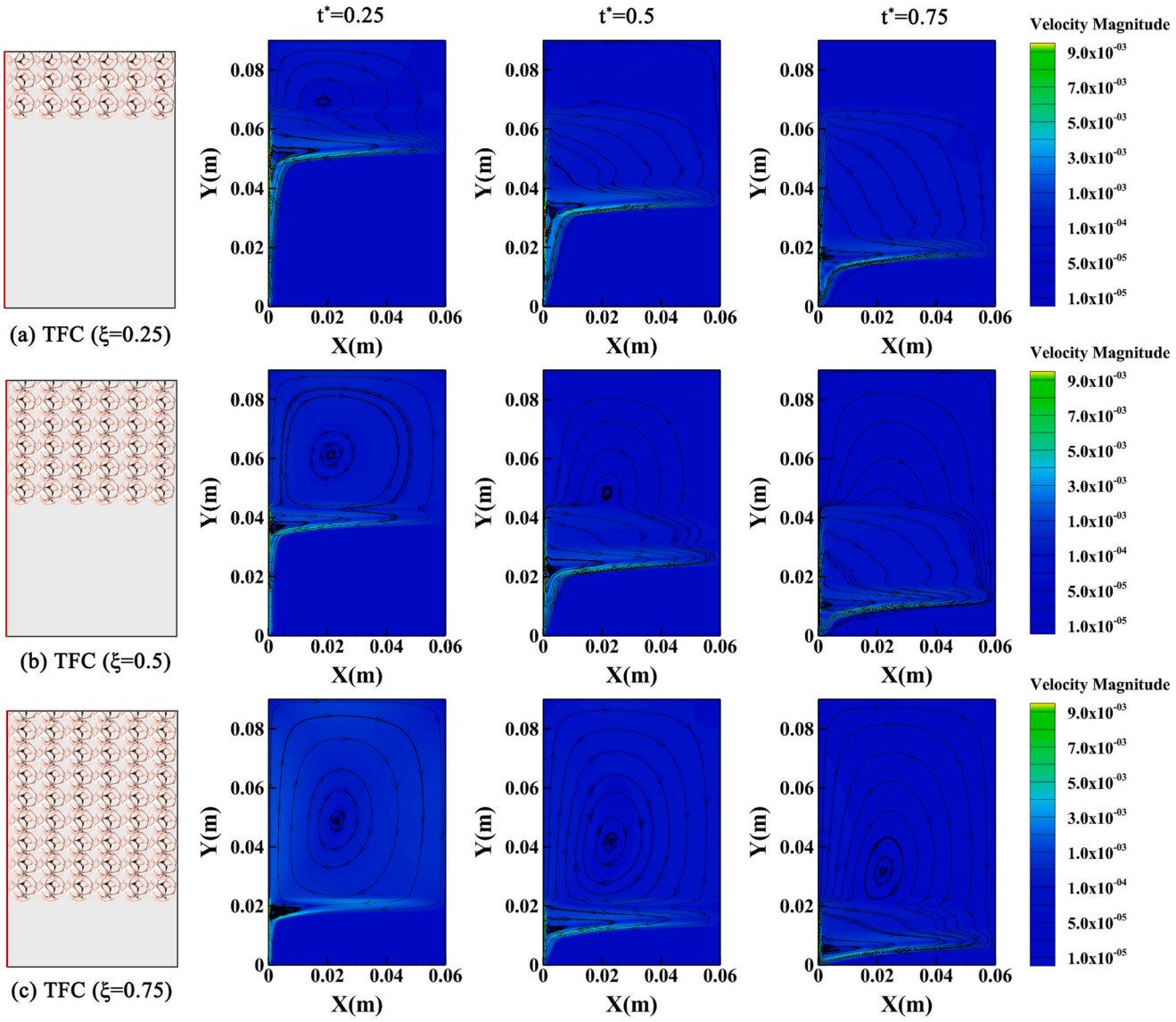

Fig. 15. Velocity field of the top filling configuration at different times. The dimensionless time is 0.25, 0.5 and 0.75, respectively.

Table 2
Order of magnitude of velocity of liquid paraffin in different regions.

	The order of magnitude of velocity (m/s)	
	Pure paraffin region	Composite region
Bottom filling	10^{-2}	10^{-3}
Top filling	10^{-3}	10^{-5}

10^{-3}m/s observed by zhang et al. [56] in pure paraffin, which can also be considered reasonable. Similarly, when the top is filled with metal foam, the liquid paraffin remains at the top. Due to the obstruction of the porous structure of the metal foam, the upward flow of the newly generated liquid paraffin in the pure paraffin region is limited. This does not help natural convection, so the overall velocity is slower. In the composite region, the order of magnitude is 10^{-5}m/s, less than 10^{-4}m/s, and the cycle is weak or even disappears (Fig. 15(a), t* = 0.5, 0.75; Fig. 15(b), t* = 0.75). In addition, it can be found that the velocity of liquid paraffin in the composite region is lower under any configuration, meaning that the metal foam impeded the flow of paraffin. The bottom filling configuration is advantageous for the enhancement of natural convection.

In addition, some interesting phenomena have been observed in this study of velocity field. As shown in Fig. 16, the distance between the center of the vortex in the composite region and the heating surface was defined as θ, and $\Delta\theta$ was defined as the deviation rate.

$$\Delta\theta = \frac{\theta_{\xi_2} - \theta_{\xi_1}}{\theta_{\xi_1}} \tag{16}$$

The subscript ξ_1, ξ_2 indicates the different height ratio of metal foam. When the metal foam filling ratio is small ($\xi = 0.25$), the vortex center is close to the heating surface. This is because the paraffin near the heating surface melts first and the heat transfer is strong. However, the vortex center gradually moves away from the heating surface with the increase of the filling ratio. This indicates that the position of intense heat transfer moves from the wall to the material center, which also verifies that the metal foam can effectively enhance the heat transfer process of PCM. For the top-filled configuration, due to the accumulation of high temperature liquid paraffin in the composite region, the position of intense heat transfer is more centered, that is, the θ is higher than that of the bottom-filled configuration. However, it can be seen from the value of $\Delta\theta$ that when the same metal foam height ratio is increased, the deviation rate of the bottom-filled configuration is larger, which is more conducive to heat transfer enhancement.

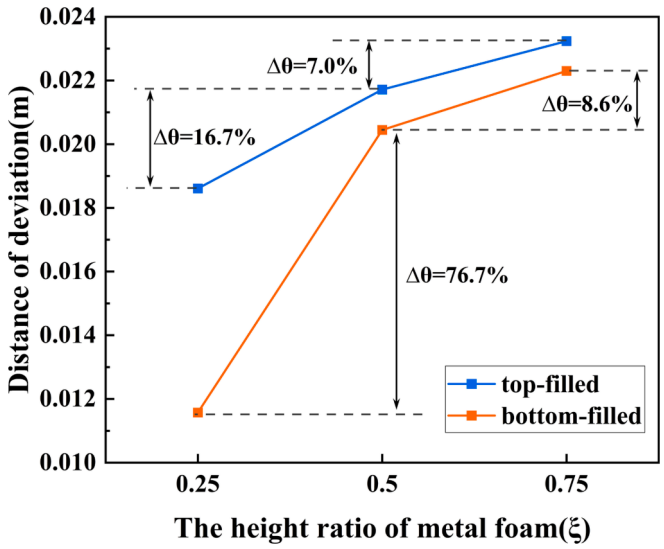

Fig. 16. The deviation distance between the vortex center and the heating surface varies with the height ratio of metal foam.

4.2. *Thermal energy storage performance*

In this paper, thermal energy storage of metal foam-paraffin composite LHTES units is defined as Eq. (17)-(21):

$$Q = Q_{pcm} + Q_{mf} \tag{17}$$

$$Q_{pcm} = Q_{la} + Q_{se} \tag{18}$$

$$Q_{la} = m_{pcm} L \tag{19}$$

$$Q_{se} = c_{p,ps} m_{pcm} (T_m - T_0) + c_{p,pl} m_{pcm} (T - T_m) \tag{20}$$

$$Q_{mf} = c_{p,mf} m_{mf} (T - T_0) \tag{21}$$

where Q_{la} is latent heat; Q_{se}, is sensible heat; $c_{p,ps}$, is the heat capacity of solid PCM; $c_{p,pl}$ is the heat capacity of liquid PCM; L is the latent heat of PCM; T_0 is the initial temperature; T_m is the phase transition temperature.

The heat storage rate is defined as Eq. (22):

$$\nu = Q/t_m \tag{22}$$

Figs. 17 and 18 presents the complete melting time and thermal energy storage rate for different cases. It can be seen from Fig. 17(a) that for the bottom-filled configuration, the melting time with ξ = 0.25, 0.5 and 0.75 are 1500 s, 999 s and 467 s, and the thermal energy storage rate are 1.26 kJ/s, 1.93 kJ/s and 4.08 kJ/s in Fig. 18(a), respectively. As ξ increases, the melting time decreases and thermal energy storage rate increases. The same pattern of variation can be observed in the top-filled configuration (Figs. 17(b) and 18(b)). However, it is worth noting that the melting time of ξ = 0.25, 0.5 and 0.75 are 2437 s, 1704 s and 913 s, and the thermal energy storage rate are 0.83 kJ/s, 1.20 kJ/s and 2.26 kJ/s, respectively. For partial filling configuration, when ξ is the same, the bottom-filled configuration melts faster and the thermal energy storage rate is higher. For partially filled configurations, when ξ = 0.75, both bottom-filled and top-filled configurations reach the shortest melting time and the highest thermal energy storage rate.

The influence of different filling configurations on thermal energy storage and average temperature are portrayed in Fig. 19. When ξ is the same, the mass of paraffin in each case is equal. So when the paraffin is completely melted, the latent heat is the same. The difference of heat storage capacity between the bottom-filled and top-filled configurations comes from the sensible heat of paraffin and metal foam. It can be seen from Eqs. (20) and (21) that sensible heat is related to temperature difference, so the change of sensible heat should be consistent with the change of the trend of the average temperature (Fig. 19). As depicted in Fig. 19(a), for the bottom-filled configuration, the thermal energy storage of ξ = 0.25, 0.5 and 0.75 are 1961.4594 kJ, 1925.26366 kJ and 1905.0215 kJ, respectively. As ξ increases from 0.25 to 0.75, heat storage decreased by 2.29%, 4.08% and 5.09%, respectively. The main reason is that with the increase of ξ, the mass of paraffin decreases, which leads to the decrease of thermal energy storage. On the other hand, with the shortening of melting time, the final temperature reached after the complete melting of composite PCM decreases, which also leads to the decrease of thermal energy storage. For ξ = 1, the thermal energy storage loss is up to 5.53% of that of the case when ξ = 0.

For the top-filled configuration, as depicted in Fig. 19(b), when ξ = 0.25, 0.5 and 0.75, the TES are 2028.1684 kJ, 2044.9843 kJ and 2064.4558 kJ, respectively. When ξ increases from 0.25 to 0.75, the heat storage increases by 0.97%, 1.72% and 2.78%. It is found that the thermal energy storage increases slightly with ξ. This is caused by its melting characteristics are different from the bottom-filled configuration. The enhanced heat transfer effect of metal foam only affects the composite region, resulting in a much longer melting time than that of the bottom-filled configuration. When ξ is the same, the final temperature reached at the completion of melting is higher in the top-filled configuration. Consequently, its thermal energy storage is higher than that of the bottom-filled configuration, and with the increase of ξ, the final temperature will further rise, leading to the increase of thermal energy storage. When ξ = 1, the melting time and thermal energy storage decrease sharply at the same time because there is no pure paraffin region.

To sum up, from Figs. 17-19, it can be concluded that the shorter melting time is at the expense of thermal energy storage, and those with

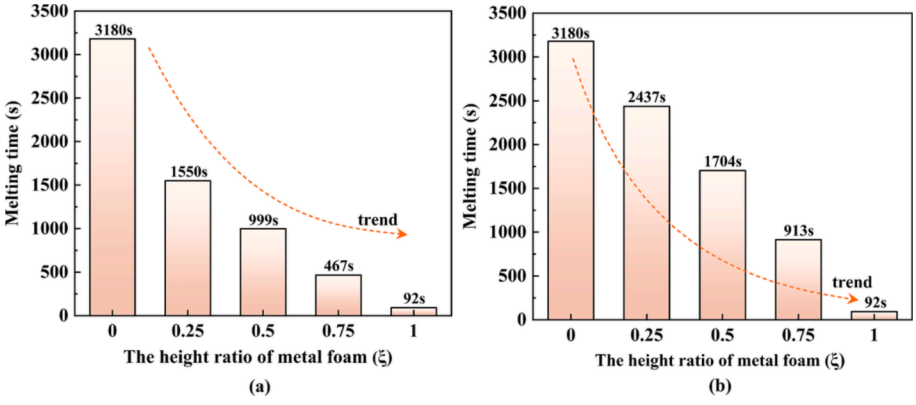

Fig. 17. Influence of the various filling heights on the complete melting time with bottom filling (a) and top filling (b) configurations.

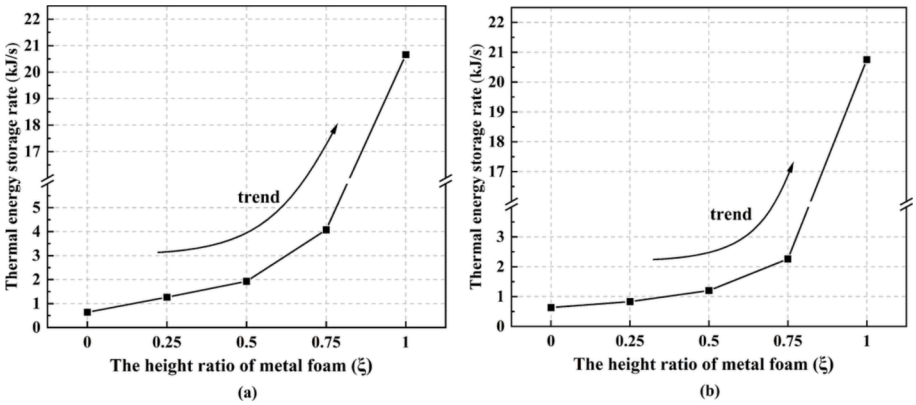

Fig. 18. Influence of the various filling heights on the thermal energy storage rate with bottom filling (a) and top filling (b) configurations.

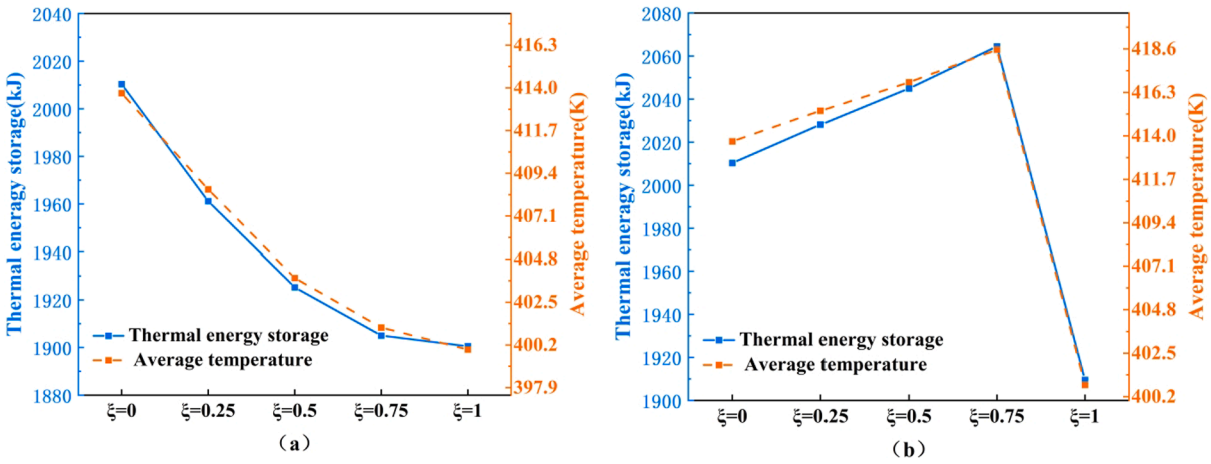

Fig. 19. Influence of the various filling heights on the TES and average temperature with bottom filling (a) and top filling (b) configurations.

more advantages in thermal energy storage have longer melting time. This is a choice that needs to be evaluated.

4.3. Economic performance

In practical engineering applications, in addition to the thermal energy storage performance of materials, economic performance is also a vital index, which determines the project cost.

The economic index P_c is defined in Eq. (23), represents the heat storage performance of materials per unit time per unit cost.

$$P_c = \frac{Q}{t_m C} \approx \frac{m_{pcm} L}{t_m (i m_{mf} + j m_{pcm})} \tag{23}$$

C is the total cost of PCM and metal foam, i and j are the unit price of metal foam and PCM respectively.

In dimensionless P_c' is defined as Eq. (24), where $P_{c,N}$ represents the case when $\xi = 0$, M is the ratio of the respective unit prices of metal foam and PCM.

$$P_c' = \frac{P_c}{P_{c,N}} = \frac{m_{pcm} L}{t_m (i m_{mf} + j m_{pcm})} \Big/ \frac{m_{pcm,N} L}{t_{m,N} j m_{pcm,N}} = \frac{m_{pcm}}{\frac{t_m}{t_{m,N}} (M m_{mf} + m_{pcm})} \tag{24}$$

The unit prices of PCM and metal foam are affected by many factors, such as the market, and are not fixed. Therefore, a fluctuation range of 10–30 is set for M. The variations of P_c' with N for different filling configurations is portrayed in Fig. 20. The top-filled configuration cases are shown as dashed lines, whereas the bottom-filled configuration cases are shown as solid lines. As can be seen from the figure, Case-B3(bottom-filled, $\xi = 0.75$) is far ahead in the whole M value range, reflecting good

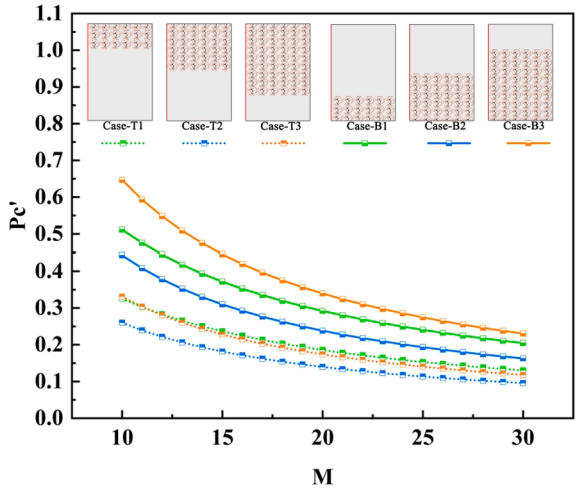

Fig. 20. Variations of the economic index P_c' with M for different filling configurations.

economy performance. The economic performance of the bottom-filled configuration is better than that of the top-filled configuration at any ξ, which can be clearly visible from the figure. For the top-filled configuration, when $\xi = 0.25$ and $\xi = 0.75$, the P_c' curves almost overlap, indicating that it is wasteful to fill the metal foam at a proportion ξ greater than 0.25. From the economic point of view, Case-B3

(bottom-filled, ξ = 0.75) is superior.

4.4. Comprehensive evaluation index

The complete melting time, thermal energy storage and total material cost determine the performance of the LHTES units. Consequently, a comprehensive strengthening goodness factor (CSGF) is proposed in this study to compare the performance of different filling configurations. The definition of CSGF is shown in Eq. (25) -(28):

$$\eta = a\eta_Q + b\eta_t + c\eta_{Pc}, a + b + c = 1; 0 \le a, b, c \le 1 \tag{25}$$

$$\eta_Q = \frac{Q}{Q_N} \tag{26}$$

$$\eta_t = \frac{t_N}{t_m} \tag{27}$$

$$\eta_{pc} = P_c^{'} \tag{28}$$

where η_Q is the dimensionless goodness factor of thermal energy storage, and is the ratio of Q to Q_N ($\xi = 0$); η_t is the dimensionless goodness factor of the complete melting time, and is the ratio of t_N ($\xi = 0$) to t_m; η_{pc} is the dimensionless goodness factor of P_c, which is defined in Eq. (23); a, b and c are the weighting coefficients. η is a constant greater than zero. The larger η is, the higher the comprehensive performance is.

When $a = b = 0$ and $c = 1$, it means that only economic factors are considered, η will be equal to P_c', which is included in CSGF as a particular condition shown in the previous section. According to the working conditions in this study, the CSGF when only considering the complete melting time (η_t), thermal energy storage (η_Q), and the same weight ($a = b = c = 1/3$) are given below. The η_t and η_Q in different cases are illustrated in Fig. 21(a) and 21(b), respectively. If the complete melting time is the only criterion in practical application, the bottom-filled configuration (ξ = 0.75) with the largest η_t can be selected as the optimum configuration. If only TES is considered, the top-filled configuration (ξ = 0.75) with the largest η_Q can be chosen as the most suitable configuration. When the three are equally focused in practice and there is no emphasis, as presented in Fig. 21(c), it is clear that the bottom-filled configuration (ξ = 0.75) has an absolute advantage. Consequently, CSGF can be used to determine the optimum filling configuration for practical applications more quickly.

5. Conclusion

In the current study, for the heat storage unit of LHTES system, two types of filling modes, top-filled and bottom-filled configurations, are designed. Meanwhile, the different filling height ratio of the metal foam is considered. The melting characteristics of different LHTES units were analyzed and a new criterion CSGF was proposed to evaluate their comprehensive performance. Conclusions can be summarized as follows:

(1) When the metal foam is filled at the bottom, the liquid paraffin has a higher flow rate, which helps to strengthen the natural convection in the pure paraffin region, improve the overall melting rate and temperature rise rate, and accelerate the melting process. However, the internal flow rate of the top filling configuration is slower, and the heat transfer enhancement is not as good as that of the bottom filling configuration, but it can achieve a higher final temperature.

(2) The top-filled configuration will increase the thermal energy storage, while the bottom-filled will significantly weaken it. The metal foam filled at the top (ξ = 0.75) has the highest thermal energy storage, compared with the fully filled one, is 7.47% higher with about 25% of the metal foam saved, which is of great practical significance for improving economic performance.

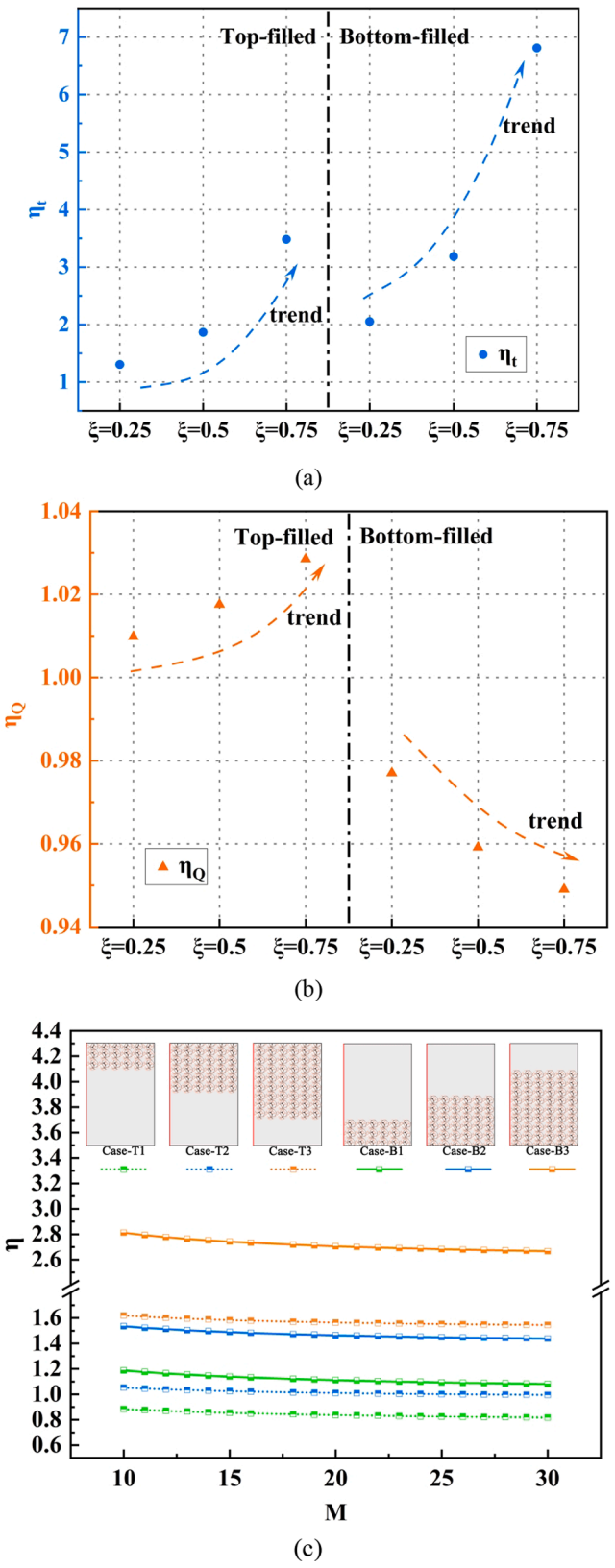

Fig. 21. Influence of the different filling configurations on the (a) η_t, (b) η_Q and (c) CSGF with M.

(3) CSGF is a new dimensionless evaluation criterion of the complete melting time, thermal energy storage and cost. Unlike previous criterions, it takes both heat storage and economy into account. Through its analysis, it is concluded that the bottom-filled configuration has the advantage in complete melting time and economy, while the top-filled configuration has the advantage in thermal energy storage.

(4) The strategy of partially filling metal foam has been proved to be effective in enhancing heat transfer, increasing thermal energy storage or reducing cost. Both the bottom and top filling config-urations have their own advantages. In future studies, the struc-ture can be further optimized and the metal foam layer with porosity gradient, material gradient and thickness gradient can be set to improve heat transfer and economic performance.

CRediT authorship contribution statement

Qifan Ying: Writing – original draft, Conceptualization, Methodology, Software, Visualization. **Hui Wang:** Writing – review & editing, Conceptualization, Project administration, Supervision. **Eric Lichtfouse:** Writing – review & editing.

Declaration of Competing Interest

The authors declare that they have no known competing financial interests or personal relationships that could have appeared to influence the work reported in this paper.

Acknowledgments

The study was funded by State Key Laboratory for Modification of Chemical Fibers and Polymer Materials, Donghua University (KF2123), Shanghai Sailing Program (19YF14011700).

References

[1] D.-K. Bui, T.N. Nguyen, A. Ghazlan, et al., Enhancing building energy efficiency by adaptive façade: a computational optimization approach [J], Appl. Energy 265 (2020), 114797.
[2] Z. Li, Y. Lu, R. Huang, et al., Applications and technological challenges for heat recovery, storage and utilisation with latent thermal energy storage [J], Appl. Energy 283 (2021), 116277.
[3] Y. Gao, X. Zhang, X. Xu, et al., Application and research progress of phase change energy storage in new energy utilization [J], J. Mol. Liq. 343 (2021), 117554.
[4] F. Javadi, H. Metselaar, P. Ganesan, Performance improvement of solar thermal systems integrated with phase change materials (PCM), a review [J], Sol. Energy 206 (2020) 330–352.
[5] W. Wu, X. Wang, M. Xia, et al., A novel composite PCM for seasonal thermal energy storage of solar water heating system [J], Renew. Energy 161 (2020) 457–469.
[6] Q. Ren, P. Guo, J. Zhu, Thermal management of electronic devices using pin-fin based cascade microencapsulated PCM/expanded graphite composite [J], Int. J. Heat Mass Transf. 149 (2020), 119199.
[7] Farzanehnia Amin, Khatibi, et al., Experimental investigation of multiwall carbon nanotube/paraffin based heat sink for electronic device thermal management [J], Energ. Conver. Manage. 179 (2019) 314–325.
[8] M.M. Heyhat, S. Mousavi, M. Siavashi, Battery thermal management with thermal energy storage composites of PCM, metal foam, fin and nanoparticle [J], J. Storage Mater. 28 (2020), 101235.
[9] A. Sciacovelli, F. Gagliardi, V. Verda, Maximization of performance of a PCM latent heat storage system with innovative fins [J], Appl. Energy 137 (2015) 707–715.
[10] C. Ji, Z. Qin, Z. Low, et al., Non-uniform heat transfer suppression to enhance PCM melting by angled fins [J], Appl. Therm. Eng. 129 (2018) 269–279.
[11] S. Yao, X. Huang, Study on solidification performance of PCM by longitudinal triangular fins in a triplex-tube thermal energy storage system [J], Energy 227 (2021), 120527.
[12] A. Arshad, M.I. Alabdullatif, M. Jabbal, et al., Towards the thermal management of electronic devices: a parametric investigation of finned heat sink filled with PCM [J], Int. Commun. Heat Mass Transfer 129 (2021), 105643.
[13] M. Bashar, K. Siddiqui, Experimental investigation of transient melting and heat transfer behavior of nanoparticle-enriched PCM in a rectangular enclosure [J], J. Storage Mater. 18 (2018) 485–497.
[14] M. Al-Jethelah, S. Ebadi, K. Venkateshwar, et al., Charging nanoparticle enhanced bio-based PCM in open cell metallic foams: an experimental investigation [J], Appl. Therm. Eng. 148 (2019) 1029–1042.
[15] P.M. Kumar, R. Anandkumar, D. Sudarvizhi, et al., Experimental and theoretical investigations on thermal conductivity of the paraffin wax using CuO nanoparticles [J], Mater. Today:. Proc. 22 (2020) 1987–1993.
[16] T. Wang, A. Almarashi, Y.A. Al-Turki, et al., Approaches for expedition of discharging of PCM involving nanoparticles and radial fins [J], J. Mol. Liq. 329 (2021), 115052.
[17] M. Mehrali, S.T. Latibari, M. Mehrali, et al., Shape-stabilized phase change materials with high thermal conductivity based on paraffin/graphene oxide composite [J], Energ. Conver. Manage. 67 (2013) 275–282.
[18] J. Yang, G.-Q. Qi, Y. Liu, et al., Hybrid graphene aerogels/phase change material composites: thermal conductivity, shape-stabilization and light-to-thermal energy storage [J], Carbon 100 (2016) 693–702.
[19] Y. Zhu, Y. Qin, S. Liang, et al., Graphene/SiO2/n-octadecane nanoencapsulated phase change material with flower like morphology, high thermal conductivity, and suppressed supercooling [J], Appl. Energy 250 (2019) 98–108.
[20] W.H. Li, S. Lai-Iskandar, D. Tan, et al., Thermal conductivity enhancement and shape stabilization of phase-change materials using three-dimensional graphene and graphene powder [J], Energy Fuel 34 (2) (2020) 2435–2444.
[21] Z. Qu, W. Li, W. Tao, Numerical model of the passive thermal management system for high-power lithium ion battery by using porous metal foam saturated with phase change material [J], Int. J. Hydrogen Energy 39 (8) (2014) 3904–3913.
[22] Y. Yao, H. Wu, Z. Liu, A new prediction model for the effective thermal conductivity of high porosity open-cell metal foams [J], Int. J. Therm. Sci. 97 (2015) 56–67.
[23] H. Wang, L. Guo, K. Chen, Theoretical and experimental advances on heat transfer and flow characteristics of metal foams [J], Sci. China Technol. Sci. 63 (5) (2020) 705–718.
[24] Z. Zhang, J. Cheng, X. He, Numerical simulation of flow and heat transfer in composite PCM on the basis of two different models of open-cell metal foam skeletons [J], Int. J. Heat Mass Transf. 112 (2017) 959–971.
[25] Y. Tian, C.Y. Zhao, A numerical investigation of heat transfer in phase change materials (PCMs) embedded in porous metals [J], Energy 36 (9) (2011) 5539–5546.
[26] Zhu z-q, huang y-k, hu n,, et al., Transient performance of a PCM-based heat sink with a partially filled metal foam: effects of the filling height ratio [J], Appl. Therm. Eng. 128 (2018) 966–972.
[27] X. Chen, X. Li, X. Xia, et al., Thermal performance of a pcm-based thermal energy storage with metal foam enhancement [J], Energies 12 (17) (2019) 3275.
[28] Y. Tang, H. Wang, C. Huang, Pore-scale numerical simulation of the heat transfer and fluid flow characteristics in metal foam under high Reynolds numbers based on tetrakaidecahedron model [J], Int. J. Therm. Sci. 184 (2023), 107903.
[29] X. Yang, X. Wang, Z. Liu, et al., Influence of aspect ratios for a tilted cavity on the melting heat transfer of phase change materials embedded in metal foam [J], Int. Commun. Heat Mass Transfer 122 (2021), 105127.
[30] S. Zhang, L. Pu, S. Mancin, et al., Experimental study on heat transfer characteristics of metal foam/paraffin composite PCMs in large cavities: Effects of material types and heating configurations [J], Appl. Energy 325 (2022), 119790.
[31] Y. Tao, Y. You, Y. He, Lattice Boltzmann simulation on phase change heat transfer in metal foams/paraffin composite phase change material [J], Appl. Therm. Eng. 93 (2016) 476–485.
[32] K. Lafdi, O. Mesalhy, S. Shaikh, Experimental study on the influence of foam porosity and pore size on the melting of phase change materials [J], J. Appl. Phys. 102 (8) (2007), 083549.
[33] B.V.S. Dinesh, A. Bhattacharya, Effect of foam geometry on heat absorption characteristics of PCM-metal foam composite thermal energy storage systems [J], Int. J. Heat Mass Transf. 134 (2019) 866–883.
[34] J.M. Mahdi, E.C. Nsofor, Multiple-segment metal foam application in the shell-and-tube PCM thermal energy storage system [J], J. Storage Mater. 20 (2018) 529–541.
[35] O. Mesalhy, K. Lafdi, A. Elgafy, et al., Numerical study for enhancing the thermal conductivity of phase change material (PCM) storage using high thermal conductivity porous matrix [J], Energ. Conver. Manage. 46 (6) (2005) 847–867.
[36] M. Caliano, N. Bianco, G. Graditi, et al., Analysis of a phase change material-based unit and of an aluminum foam/phase change material composite-based unit for cold thermal energy storage by numerical simulation [J], Appl. Energy 256 (2019), 113921.
[37] S. Zhang, L. Pu, S. Mancin, et al., Role of partial and gradient filling strategies of copper foam on latent thermal energy storage: an experimental study [J], Energy 255 (2022), 124517.
[38] Y. Xu, Q. Ren, Zheng z-j,, et al., Evaluation and optimization of melting performance for a latent heat thermal energy storage unit partially filled with porous media [J], Appl. Energy 193 (2017) 84–95.
[39] V. Joshi, M.K. Rathod, Thermal performance augmentation of metal foam infused phase change material using a partial filling strategy: an evaluation for fill height ratio and porosity [J], Appl. Energy 253 (2019).
[40] Z. Wang, H. Zhang, B. Dou, et al., Effect of copper metal foam proportion on heat transfer enhancement in the melting process of phase change materials [J], Appl. Therm. Eng. 201 (2022), 117778.
[41] Y. Xu, M.J. Li, Z.J. Zheng, et al., Melting performance enhancement of phase change material by a limited amount of metal foam: Configurational optimization and economic assessment [J], Appl. Energy 212 (FEB.15) (2018) 868–880.
[42] X. Lou, H. Wang, H. Xiang, Solidification performance enhancement of encapsulated ice storage system by fins and copper foam [J], Int. J. Refrig 134 (2022) 293–303.
[43] H. Zuo, M. Wu, K. Zeng, et al., Numerical investigation and optimal design of partially filled sectorial metal foam configuration in horizontal latent heat storage unit [J], Energy 237 (2021), 121640.

[44] Y. Tian, Zhao c-y., A numerical investigation of heat transfer in phase change materials (PCMs) embedded in porous metals [J], Energy 36 (9) (2011) 5539–5546.
[45] M. Esapour, A. Hamzehnezhad, A.A.R. Darzi, et al., Melting and solidification of PCM embedded in porous metal foam in horizontal multi-tube heat storage system [J], Energ. Conver. Manage. 171 (2018) 398–410.
[46] V. Shatikian, G. Ziskind, R. Letan, Numerical investigation of a PCM-based heat sink with internal fins [J], Int. J. Heat Mass Transf. 48 (17) (2005) 3689–3706.
[47] H. Zheng, C. Wang, Q. Liu, et al., Thermal performance of copper foam/paraffin composite phase change material [J], Energ. Conver. Manage. 157 (2018) 372–381.
[48] A. Chamkha, A. Veismoradi, M. Ghalambaz, et al., Phase change heat transfer in an L-shape heatsink occupied with paraffin-copper metal foam [J], Appl. Therm. Eng. 177 (2020), 115493.
[49] A A V A, B A S M, Numerical study on melting of paraffin wax with Al2O3 in a square enclosure - ScienceDirect [J], Int. Commun. Heat Mass Transfer 39(1) (2012) 8-16.
[50] J.G. Fourie, J.P. du Plessis, Pressure drop modelling in cellular metallic foams [J], Chem. Eng. Sci. 57 (14) (2002) 2781–2789.
[51] V.V. Calmidi, Transport phenomena in high porosity fibrous metal foams [M], University of Colorado at Boulder, 1998.
[52] A. Bhattacharya, V.V. Calmidi, R.L. Mahajan, Thermophysical properties of high porosity metal foams [J], Int. J. Heat Mass Transf. 45 (5) (2002) 1017–1031.
[53] Zheng z-j, yang c, xu y,, et al., Effect of metal foam with two-dimensional porosity gradient on melting behavior in a rectangular cavity [J], Renew. Energy 172 (2021) 802–815.
[54] W. Li, Z. Qu, Y. He, et al., Experimental and numerical studies on melting phase change heat transfer in open-cell metallic foams filled with paraffin [J], Appl. Therm. Eng. 37 (2012) 1–9.
[55] Y. Tian, C. Zhao, Thermal and exergetic analysis of metal foam-enhanced cascaded thermal energy storage (MF-CTES) [J], Int. J. Heat Mass Transf. 58 (1–2) (2013) 86–96.
[56] P. Zhang, Z. Meng, H. Zhu, et al., Melting heat transfer characteristics of a composite phase change material fabricated by paraffin and metal foam [J], Appl. Energy 185 (2017) 1971–1983.